EDGE ARTICLE

CsPbBr₃–CdS heterostructure: stabilizing perovskite nanocrystals for photocatalysis†

Anthony Kipkorir,[ab] Jeffrey DuBose, [ORCID][ab] Junsang Cho[a] and Prashant V. Kamat [ORCID] ⋆[abc]

The instability of cesium lead bromide (CsPbBr₃) nanocrystals (NCs) in polar solvents has hampered their use in photocatalysis. We have now succeeded in synthesizing CsPbBr₃–CdS heterostructures with improved stability and photocatalytic performance. While the CdS deposition provides solvent stability, the parent CsPbBr₃ in the heterostructure harvests photons to generate charge carriers. This heterostructure exhibits longer emission lifetime (τ_{ave} = 47 ns) than pristine CsPbBr₃ (τ_{ave} = 7 ns), indicating passivation of surface defects. We employed ethyl viologen (EV^{2+}) as a probe molecule to elucidate excited state interactions and interfacial electron transfer of CsPbBr₃–CdS NCs in toluene/ethanol mixed solvent. The electron transfer rate constant as obtained from transient absorption spectroscopy was 9.5×10^{10} s^{-1} and the quantum efficiency of ethyl viologen reduction ($\Phi_{EV^{+\cdot}}$) was found to be 8.4% under visible light excitation. The Fermi level equilibration between CsPbBr₃–CdS and EV^{2+}/EV$^{+\cdot}$ redox couple has allowed us to estimate the apparent conduction band energy of the heterostructure as −0.365 V *vs.* NHE. The insights into effective utilization of perovskite nanocrystals built around a quasi-type II heterostructures pave the way towards effective utilization in photocatalytic reduction and oxidation processes.

Introduction

Semiconductor quantum dots are excellent building blocks for designing light-harvesting assemblies.[1,2] The ability to chemically modify the surface with a functionalized ligand or to couple with another semiconductor particle offers a variety of ways to harvest visible photons.[3–5] Since the 1990s, metal chalcogenide quantum dots (QDs), CdSe in particular, have served as the prototypical compound to elucidate excited state and charge transfer properties.[6–8] In recent years, another quantum dot system, *viz.*, perovskite nanocrystals (CsPbX₃, X = Cl, Br, I), has emerged as a model semiconductor QD system to probe light induced optoelectronic and photocatalytic properties.[9–13] We have recently elucidated the photocatalytic aspects of CsPbBr₃ QDs by probing the interfacial electron transfer to methyl viologen[14,15] and ferrocenium cation.[16] To date, the use of these perovskite quantum dots in photocatalysis has been limited only to a few nonpolar solvents.[17–21] The weakly-binding organic ligand shell around perovskite nanocrystals does not provide sufficient stability in polar solvents. In order to expand the scope of the perovskite nanocrystals to a wide range of

photocatalytic applications (*e.g.*, solar hydrogen production or CO₂ reduction), it is important to provide protection against chemical transformation in the presence of a redox couple or in a polar medium.

One simple approach to achieve stability in polar solvents is to cap the semiconductor nanocrystals with a thin inorganic shell. Design of such heterostructures has been successfully employed for binary and ternary semiconductors like CdSe/ZnS,[22,23] InP/ZnS,[24] and AgInS₂/ZnS.[25] The heterostructure with type I or type II band alignment offers strategies to enhance emission of the core QD or improve charge separation within the heterostructure. Although a few reports exist to-date of capping CsPbBr₃ QDs with SiO₂,[26] CdS,[27] or ZnS[28,29] shells, none of these heterostructures have shown a major leap in achieving improved performance with a long-term stability in polar solvents. Ambiguity still exists whether the added material forms a continuous shell around the perovskite core or forms smaller discontinuous islands on the surface.[26] Given the difficulty in imaging the thin inorganic shell around perovskite nanocrystals, because of the image contrast, one employs stability tests in a polar medium or its resistance to halide exchange to confirm surface modification.[30–33]

Designing perovskite heterostructures with metal chalcogenide shells can have several distinct advantages: (i) providing stability towards increased polarity of the solvent, (ii) remediating surface defects by directly interacting with the vacancies, and (iii) allowing for type I or quasi-type II band alignment to promote increased charge recombination in the core (increased emission yield) or improved charge separation.[34–36]

[a]*Radiation Laboratory, University of Notre Dame, Notre Dame, Indiana 46556, USA*

[b]*Department of Chemistry and Biochemistry, University of Notre Dame, Notre Dame, Indiana 46556, USA*

[c]*Department of Chemical and Biomolecular Engineering, University of Notre Dame, Notre Dame, Indiana 46556, USA. E-mail: pkamat@nd.edu*

† Electronic supplementary information (ESI) available: The ESI includes experimental methods and procedures, actinometry, data of control experiments and kinetic analysis. See DOI: 10.1039/d1sc04305f

In this context, a $CsPbBr_3$–CdS heterostructure offers an attractive means to tune the band energies, as their conduction bands are nearly isoenergetic (E_{CB} of $CsPbBr_3$ and quantized CdS ≈ −0.8 V versus NHE)[37–39] and facilitate charge separation. In addition, cubic $CsPbBr_3$ nanocrystals have a lattice constant (*a*) of 5.85 Å (ref. 40) while that of CdS (zinc blende structure) is 5.83 Å.[41] The similarity of the two values signifies the possibility of having a less strained interface with reduced defect states.[42] We have now successfully prepared $CsPbBr_3$–CdS heterostructures in a two-step method, and the optical properties of these structures are discussed.

Results and discussion

$CsPbBr_3$–CdS heterostructure

$CsPbBr_3$ quantum dots (QDs) dispersed in octadecene (ODE) were prepared using a previously reported procedure.[43] These QDs were then treated with cadmium diethyldithiocarbamate ($Cd(DDTC)_2$) at 110 °C to obtain CdS capped $CsPbBr_3$ QDs. Experimental details on the synthesis of $CsPbBr_3$ and $CsPbBr_3$–CdS QDs are presented in the ESI (Fig. S1†). The transmission electron microscopy (TEM) images of the two nanocrystals are shown in Fig. 1A and B. These cubic particles are similar in size showing particles of lengths 8–9 nm (see Fig. S2† for size distribution analysis). This shows that CdS capping in the heterostructure is relatively thin compared to the $CsPbBr_3$ core and it is difficult to identify with the image contrast in TEM images. This observation is consistent with earlier work which reports difficulty in characterizing the shell in a $CsPbBr_3$ heterostructure using TEM analysis.[44,45] These studies have attributed the imaging difficulty to low electron density contrast of the shell. However, other techniques such as elemental analysis can be useful to overcome these limitations.

We succeeded in establishing the presence of CdS in the $CsPbBr_3$–CdS heterostructures through elemental analysis with TEM energy dispersive X-ray (EDX) spectroscopy. Fig. 1C–G which present elemental mapping, confirm the presence of Cd and S along with Cs, Pb, and Br. The elemental ratio (Fig. 1H) also suggests a relatively low concentration of CdS as compared to Cs, Pb and Br in the heterostructure. We can conclude that any CdS in the heterostructure is of the order of a monolayer. However, there is also the possibility of forming small clusters in and around the $CsPbBr_3$ QDs.

Evidence of surface modification with CdS was also seen through the change in the surface charge. Zeta potential measurements indicated that $CsPbBr_3$–CdS QDs suspended in toluene carry more negative surface charge (−37.4 mV) than pristine $CsPbBr_3$ nanocrystals in toluene (−15.8 mV). This increased surface charge of $CsPbBr_3$–CdS QDs enabled us to carry out electrophoretic deposition of a film under the influence of a DC field (see ESI† for details; Fig. S3†). The increased surface negativity and ability to be deposited as a film under applied bias indicates a modified surface around $CsPbBr_3$. Similar electrophoretic deposition was also possible when $CsPbBr_3$ nanocrystals were coated with a $PbSO_4$–oleate shell.[46] It should be noted that pristine $CsPbBr_3$ QDs suspended in toluene cannot be deposited as film using electrophoresis as it does not carry sufficient surface charge.

In addition to $CsPbBr_3$ and $CsPbBr_3$–CdS heterostructures, we also synthesized CdS QDs with the same ligands following a similar experimental procedure (i.e. without $CsPbBr_3$). Fig. 2A shows the absorption spectra of $CsPbBr_3$, CdS and $CsPbBr_3$–CdS QDs in toluene. The CdS and $CsPbBr_3$ QDs exhibit characteristic excitonic peaks at 434 and 518 nm, respectively. Although the absorption spectrum of the $CsPbBr_3$–CdS heterostructure shows two peaks that overlap with the absorption of individual QDs, the peak around 434 nm may also arise from the deposition of small size CdS particles on the surface of $CsPbBr_3$ nanocrystals. Such a decoration of CdS particles, if any, would give rise to a CdS excitonic peak in the heterostructures. The excitonic peak at 518 nm ($CsPbBr_3$) remains unaffected after heterostructure formation, thus ruling out any interference of exchange of metal ions. Similarly, the tail absorption at longer wavelengths arises from the scattering effects, similar to what is seen in $PbSO_4$–oleate capped $CsPbBr_3$.[46]

The emission spectra of these three nanostructures are shown in Fig. 2B. Whereas CdS QDs remain the least emissive, both $CsPbBr_3$ and $CsPbBr_3$–CdS QDs are highly emissive. Additionally, the emission features of $CsPbBr_3$ QDs remain unchanged following the deposition of CdS: the emission maximum (521 nm) and the full width at half maximum (18 nm) of $CsPbBr_3$ are unaffected after CdS modification. These results confirm that there is no substitution of cations during the heterostructures synthesis, and thus the emission characteristics of the parent $CsPbBr_3$ QDs are retained in the heterostructure. If there was any substitution of Pb^{2+} with Cd^{2+} we would expect a blue shift in the absorption and emission maxima of the perovskite QD.[47] The excitation spectra recorded at different emission wavelengths confirm the origin of the emission to arise from the $CsPbBr_3$ (Fig. S4 in the ESI†).

Another interesting aspect of the capping with CdS is the enhancement in emission yield. The emission quantum yields as determined using an integrating sphere were 39% and 60% for $CsPbBr_3$ and $CsPbBr_3$–CdS QDs, respectively (see ESI† for details). Passivation of surface defects by CdS is expected to suppress nonradiative processes and thus lead to increased emission yield. For example, capping of CdSe with CdS has resulted in the significant enhancement of emission yield.[48–51] The flow of charge carriers from the CdS shell to CdSe core in these studies was established through emission and excitation spectral measurements. Control experiments were carried out to check whether introduction of Cd^{2+} ions alone can induce similar changes in the emission properties. Fig. S5† shows a decrease in emission yield and lifetime when $CsPbBr_3$ was treated with cadmium acetylacetonate ($Cd(acac)_2$) instead of $Cd(DDTC)_2$. Additionally, treatment with Cd^{2+} did not change the absorption of the QDs. This further confirms that the observed optical properties are due to the presence of CdS in the heterostructure.

We employed time-resolved emission measurements to monitor the excited state behavior of $CsPbBr_3$ before and after CdS deposition. The emission decay at 520 nm was monitored for $CsPbBr_3$ and $CsPbBr_3$–CdS samples (Fig. 2C). Each trace was
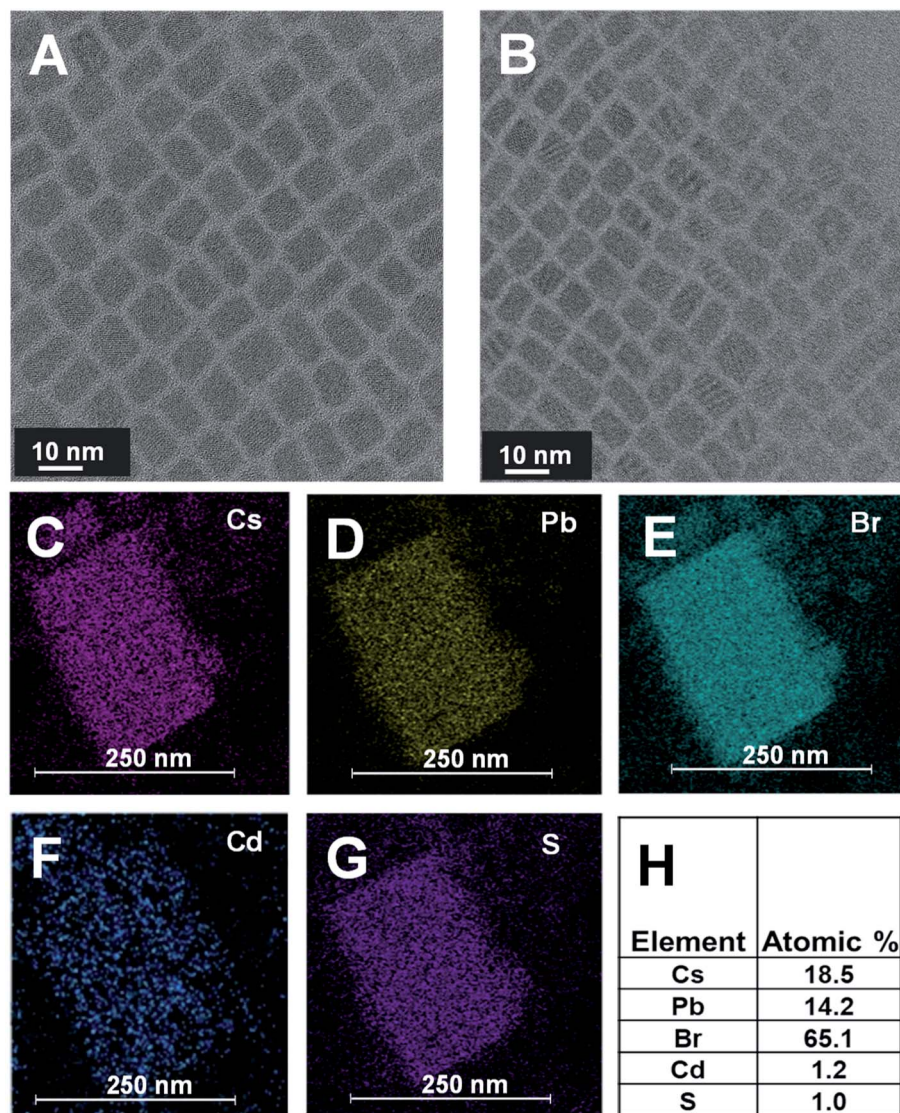
Fig. 1 TEM image for (A) pristine $CsPbBr_3$ and (B) $CsPbBr_3$–CdS. (C–G) Elemental maps showing presence of Cs, Pb, Br, Cd, and S, respectively. (H) Atomic percentage of different elements as measured by EDAX.

analyzed using a biexponential decay fit and the fitting parameters are presented in Table S1.† Of interest is the increase in emission lifetime of $CsPbBr_3$ upon capping with CdS. A nearly seven-fold increase in average lifetime of $CsPbBr_3$–CdS QDs (τ_{ave} = 46.9 ns) was observed over that of pristine $CsPbBr_3$ QDs (τ_{ave} = 7.0 ns). This shows that CdS deposition facilitates long-lived charge separation in $CsPbBr_3$–CdS. In addition to surface passivation, we can also expect the formation of a quasi-type II heterojunction as shown in the scheme (Fig. 2D). Whereas direct charge carrier recombination is dominant in pristine $CsPbBr_3$, the nearly isoenergetic conduction bands of $CsPbBr_3$ and CdS can facilitate delocalization of electrons across the two semiconductors, thus improving charge separation. Since the CdS layer is relatively thin, its contribution to the emission is expected to be small. The excitation spectra (Fig. S4†) rule out the contribution from CdS to overall emission. The observed increase in lifetime

parallels the emission yield enhancement seen in the $CsPbBr_3$–CdS heterostructure.

Stability in polar environment

Attaining long term stability of $CsPbBr_3$ nanocrystals in polar solvents remains a challenge. $CsPbBr_3$ nanocrystals undergo rapid degradation in polar solvents, which has hampered their applications in photocatalysis. Even the addition of a small amount of polar solvents such as ethanol or water can induce chemical transformation/precipitation of $CsPbBr_3$ QDs and thus a loss of photoactivity.[9,52,53] Recently, it was reported that ZnS-capped $CsPbBr_3$ QDs were stable in a toluene : water biphasic mixture. The contact with water was made by periodic shaking since the two solvents are immiscible.[28] We also conducted a similar stability test of $CsPbBr_3$ and $CsPbBr_3$–CdS nanocrystals using a biphasic mixture of toluene and water with periodic shaking. The emission spectra of $CsPbBr_3$ and
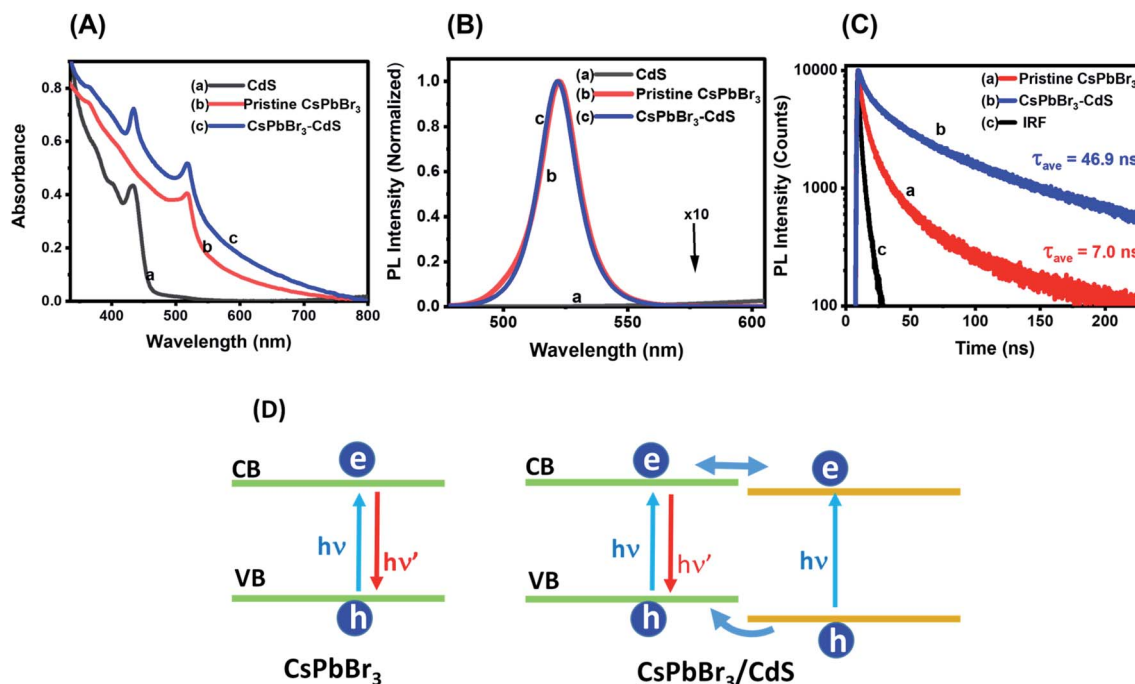
Fig. 2   (A) Absorption spectra and (B) corresponding photoluminescence (PL) spectra of (a) CdS, (b) pristine $CsPbBr_3$ and (c) $CsPbBr_3$–CdS QD suspension in toluene. (C) PL decay traces monitored at 520 nm using 370 nm excitation: (a) pristine $CsPbBr_3$ and (b) $CsPbBr_3$–CdS nanocrystal suspensions in toluene, and (c) instrument response (IRF). The kinetic analysis is presented in the ESI.† (D) Schematic diagram illustrating charge separation and charge recombination in $CsPbBr_3$ and $CsPbBr_3$–CdS nanocrystals.

$CsPbBr_3$–CdS nanocrystals and the PL intensity variation recorded during 30 hour period are shown in Fig. S6.† $CsPbBr_3$ nanocrystals became non emissive after 20 hours of exposure in biphasic mixture. On the other hand, $CsPbBr_3$–CdS nanocrystals, after an initial drop in photoluminescence, maintained more than 40% emission even after 30 hours.

The biphasic solvent mixture approach does not represent an increase in the overall polarity of the medium. Ideally, an inorganic shell should prevent direct contact of $CsPbBr_3$ with a polar environment and maintain its photostability. We checked the stability of $CsPbBr_3$ and $CsPbBr_3$–CdS by introducing a miscible polar solvent (ethanol) to a toluene suspension of the QDs and monitoring the absorption and emission spectra over time. Fig. 3A and B show the absorption and emission spectra recorded following addition of ethanol (15% v/v) to toluene solution over a period of 60 minutes. The absorption of pristine $CsPbBr_3$ QDs shows enhanced absorbance with time due to scattering effects caused by turbidity as the ligands from QD surface become detached in the polar medium.[54] A ∼85% decrease in the $CsPbBr_3$ emission yield is seen immediately after the addition of ethanol to the toluene solution. In addition, upon exposure to ethanol we also see a change in the absorption of $CsPbBr_3$ due to particle aggregation. These results confirm the susceptibility of $CsPbBr_3$ QDs to polar environment (Fig. 3C). On the other hand, $CsPbBr_3$–CdS QDs exhibit only a small decrease (∼15%) in emission with a relatively small change in the absorption during 60 min of exposure in toluene/ethanol mixed solvent. The CdS deposition

provides the necessary protection for $CsPbBr_3$, and thus decreases its susceptibility to ethanol-induced degradation.

Excited state interactions with an electron acceptor

Since $CsPbBr_3$–CdS QDs were stable in toluene/ethanol mixed solvent, we were able to probe the excited state interactions and interfacial electron transfer with a cationic electron acceptor, ethyl viologen, EV^{2+}. Emission spectra recorded at different concentrations of EV^{2+} are shown in Fig. 4A. The quenching of photoluminescence confirmed the excited state interaction between $CsPbBr_3$–CdS QDs and EV^{2+}. As a control, we tested the solubility of EV^{2+} in the toluene/ethanol mixed solvent separately by recording absorption spectra and confirming the probe molecules are fully soluble at the concentrations employed in this study (Fig. S7†). Earlier studies have shown direct complexation between $CsPbBr_3$ and methyl viologen and elucidated the role of surface bound ligands in dictating the complexation constant.[14,15] Here, we were able to quench the emission at micromolar concentrations of EV^{2+}, thus indicating a complex formation in the ground state between $CsPbBr_3$–CdS and EV^{2+}.[51] The equilibrium of the bound and unbound EV^{2+} molecules (reaction (1)) can be expressed in terms of the apparent association constant, K_{app} and emission yields (expression (2)).[55] The observed quantum yield (ϕ_f(obs)) takes into account the emission arising from EV^{2+}-bound (ϕ_f') and pristine (ϕ_f^0) $CsPbBr_3$ QDs. With increasing concentration of EV^{2+}, more $CsPbBr_3$–CdS QDs bind to viologen and thus exhibit a decrease in the emission yield.
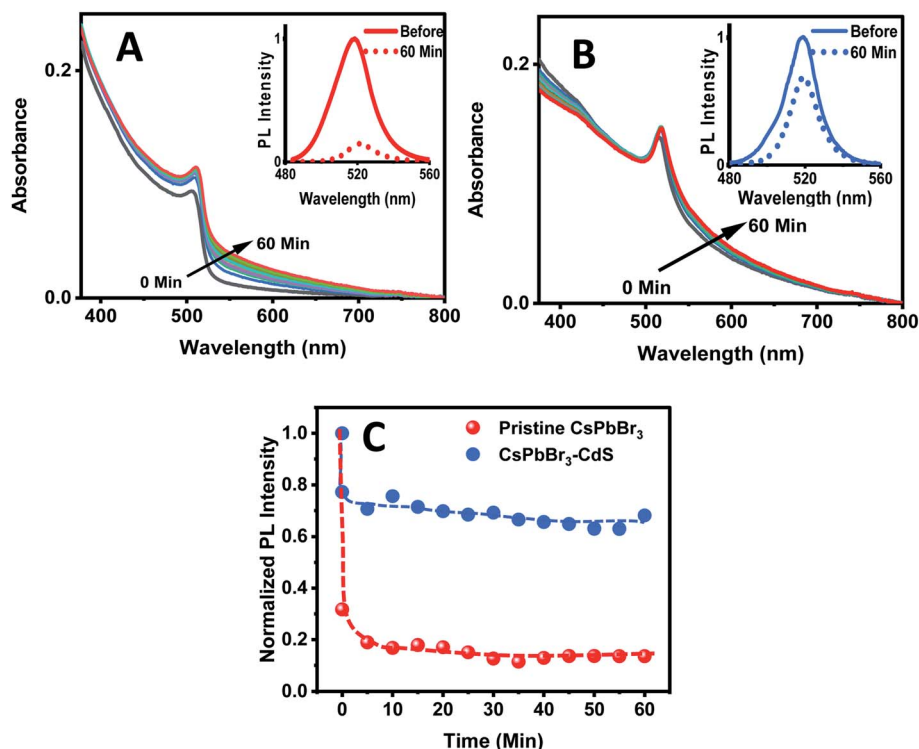
Fig. 3 Absorption spectra of (A) CsPbBr$_3$ and (B) CsPbBr$_3$–CdS QDs in toluene recorded at different time intervals after addition of ethanol (15% v/v). Spectra were recorded at a time interval of 5 min. Insets: PL spectra of QDs before and 60 min after ethanol addition (excitation: 370 nm). (C) Changes in the normalized PL intensity of the CsPbBr$_3$ and CsPbBr$_3$–CdS QDs monitored at 520 nm as a function of time after addition of ethanol (15% v/v) to the toluene suspension.

$$CsPbBr_3-CdS \ + \ EV^{2+} \ \underset{}{\overset{K_{app}}{\rightleftharpoons}} \ [CsPbBr_3-CdS\cdots EV^{2+}] \quad (1)$$

$$\frac{1}{\left(\phi_f^0 - \phi_f(obs)\right)} = \frac{1}{\left(\phi_f^0 - \phi_f'\right)} + \frac{1}{K_{app}\left(\phi_f^0 - \phi_f'\right)\left[EV^{2+}\right]} \quad (2)$$

The photoluminescence quenching data was analyzed using expression (2). The emission intensity of the QDs at the emission maximum (which is proportional to quantum yield, (ϕ_f(obs))) was monitored at different concentration of EV^{2+}.[55,56] The linear dependence of the double reciprocal plot ($1/(\phi_f^0 - \phi_f(obs))$ *versus* $1/[EV^{2+}]$) in Fig. 4B confirms the validity of the association between CsPbBr$_3$–CdS and EV^{2+}. The apparent association constant K_{app} determined from the slope and intercept of the plot in Fig. 4B was 7.0×10^4 M^{-1}. This complexation constant is 1–2 orders of magnitude smaller than the one observed for uncapped CsPbBr$_3$ and viologen (0.8–7.0×10^6 M^{-1}).[15] The decrease in K_{app} further indicates that the presence of CdS reduces the surface interactions with the viologen. The K_{app} value we obtain in this study is in line with literature values of CdS interacting with viologens.[57]

To further establish the excited state interactions, we monitored the photoluminescence lifetime of the CsPbBr$_3$–CdS QDs at different EV^{2+} concentrations. Time-resolved luminescence decay traces were recorded in toluene : ethanol (85 : 15 v/v) using an excitation source at 370 nm. The lifetimes were fitted to a biexponential kinetic expression (expression 3), and the fitting parameters are given in Table S2.†

$$y = A_1 e^{-t/\tau_1} + A_2 e^{-t/\tau_2} \quad (3)$$

The average lifetime (τ_{ave}) decreased with increasing concentration of EV^{2+} in accordance with the photoluminescence quenching seen in Fig. 4A. The decrease in average lifetime from 42.4 ns to 18.1 ns upon addition of 12 μM EV^{2+} is indicative of a competing excited state deactivation pathway involving electron transfer from the CsPbBr$_3$–CdS QDs to EV^{2+}. Since this electron transfer is likely to occur within the time resolution (~1 ns) of our photoluminescence lifetime set up, we employed femtosecond transient absorption spectroscopy to resolve the electron transfer process.

Transient absorption spectra were recorded following laser pulse excitation at 400 nm (16 μJ cm^{-2}). The transient absorption spectra of a representative CsPbBr$_3$–CdS QD sample containing 0 and 4 μM EV^{2+} are shown in Fig. 5A and B respectively. The negative absorption (exciton bleach) feature centered at ~527 nm corresponds to the charge separated state within the NCs.[58–60] The charge separation which occurs within the laser pulse is seen in spectrum 'a' recorded with a probe delay of 1 ps. As electrons and holes recombine, a recovery in the bleached absorption is seen. The bleach recovery at 527 nm for the samples containing different amounts of EV^{2+} are presented in Fig. 5C (see Fig. S8† for longer time scale kinetics). With
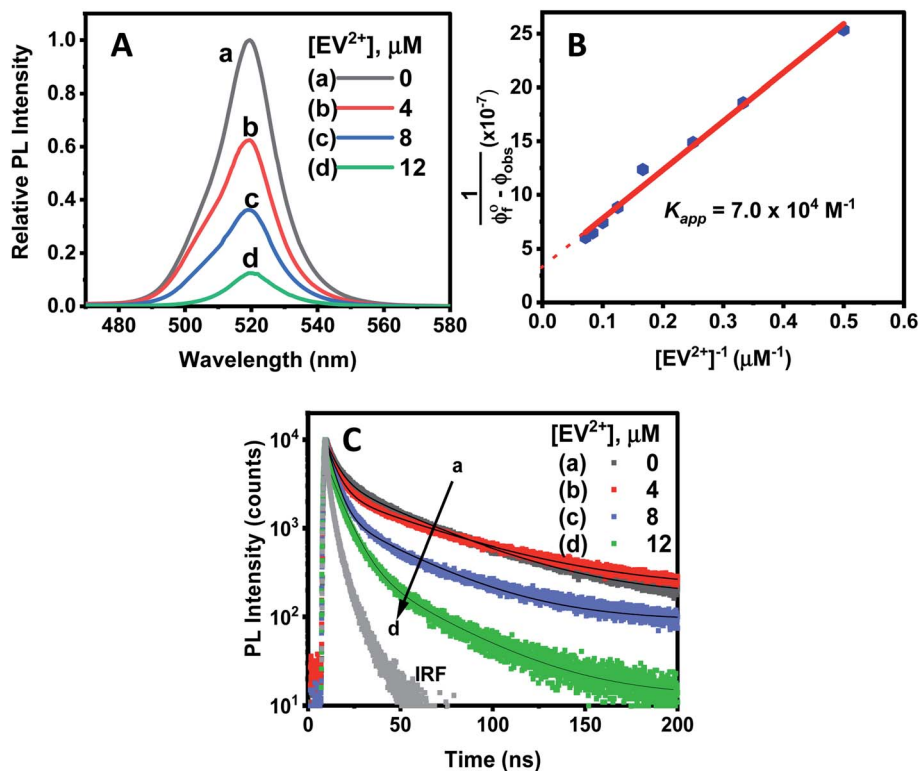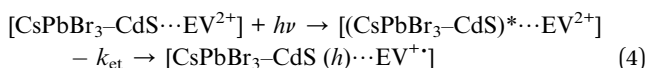
Fig. 4 (A) PL quenching of CsPbBr$_3$–CdS QDs ($\approx$16 nM) in toluene : ethanol (90 : 10% v/v) upon additions of increasing concentration of ethyl viologen (EV^{2+}) dissolved in ethanol. (B) Double reciprocal plot analysis of emission quenching of CsPbBr$_3$–CdS in toluene : ethanol. The slope (3.3 × 10^{-7}) and intercept (4.3 × 10^{-12} M^{-1}) was used to determine the apparent association constant, K_{app}, 7.0 ($\pm$0.8) × 10^4 M^{-1}. (C) Photo-luminescence decay at different EV^{2+} concentrations, recorded with 370 nm excitation and monitored at λ_{max} = 520 nm.

increasing EV^{2+} concentration we observe a quick recovery of the bleach feature, thus confirming the presence of an additional deactivation pathway for the photogenerated electrons, *viz.*, electron transfer to EV^{2+} (reaction (4)).

$$[CsPbBr_3–CdS\cdots EV^{2+}] + h\nu \rightarrow [(CsPbBr_3–CdS)^*\cdots EV^{2+}]$$
$$- k_{et} \rightarrow [CsPbBr_3–CdS\,(h)\cdots EV^{+\bullet}] \quad (4)$$

The bleach recovery was analyzed using a biexponential kinetic fit[35] and the fitting parameters (a_1, τ_1) and (a_2, τ_2) corresponding to fast and slow components are presented in Table S3.† While the fast component varied in the range 18.6–6.6 ps the long component varied in the range of 129.6–71.7 ps.

If we assign the decrease in the fast component to the electron transfer pathway from CsPbBr$_3$–CdS to EV^{2+}, we can obtain the rate constant for electron transfer through the expression (5).

$$k_{et} = \frac{1}{\tau_1\,(CsPbBr_3-CdS-EV^{2+})} - \frac{1}{\tau_1\,(CsPbBr_3-CdS)} \quad (5)$$

If we substitute the fast time components (τ_1) of CsPbBr$_3$–CdS and that of CsPbBr$_3$–CdS with 32 μM EV^{2+} in expression 5 (Table S3†), we obtain rate constant (k_{et}) of the electron transfer in the range of 3.8–9.8 × 10^{10} s^{-1} for three different EV^{2+}

concentrations (4–32 μM) or an average rate constant of 6.5 × 10^{10} s^{-1}. This rate constant for electron transfer is lower than the one obtained for electron transfer between oleic acid/oleylamine capped CsPbBr$_3$ QDs and viologen (k_{et} = 3.6 × 10^{11} s^{-1}).[15] As discussed in the emission quenching experiments, the surface interactions play a role in dictating the kinetics of interfacial electron transfer.

It is evident that modification of CsPbBr$_3$ with CdS slows down the electron transfer rate. Schemes 1A and B illustrate the two scenarios for achieving electron transfer, *viz.*, without and with CdS modification. As shown earlier, when methyl viologen is directly bound to CsPbBr$_3$, the charge separation is extended, with electrons residing in the viologen moiety and holes residing within the CsPbBr$_3$ QDs.[14] This extended charge separation as a bound pair was manifested as a long-lived transient bleach component. In contrast, the electron transfer with CsPbBr$_3$–CdS is mediated through the CdS layer as expected by the quasi-type II band alignment (Scheme 1C). The reduced ethyl viologen (EV$^{+\bullet}$) is no longer directly bound to the CsPbBr$_3$, but instead is now linked to the CdS layer. Similar CdS-mediated electron transfer has been observed in CdSe–CdS heterostructures.[51] The bleaching recovery accelerates with increasing viologen concentrations as the electrons are depleted from the CsPbBr$_3$ core, mediated through CdS. The distinct difference between the two bleach recovery kinetics observed with pristine CsPbBr$_3$ and CsPbBr$_3$–CdS QDs further highlights
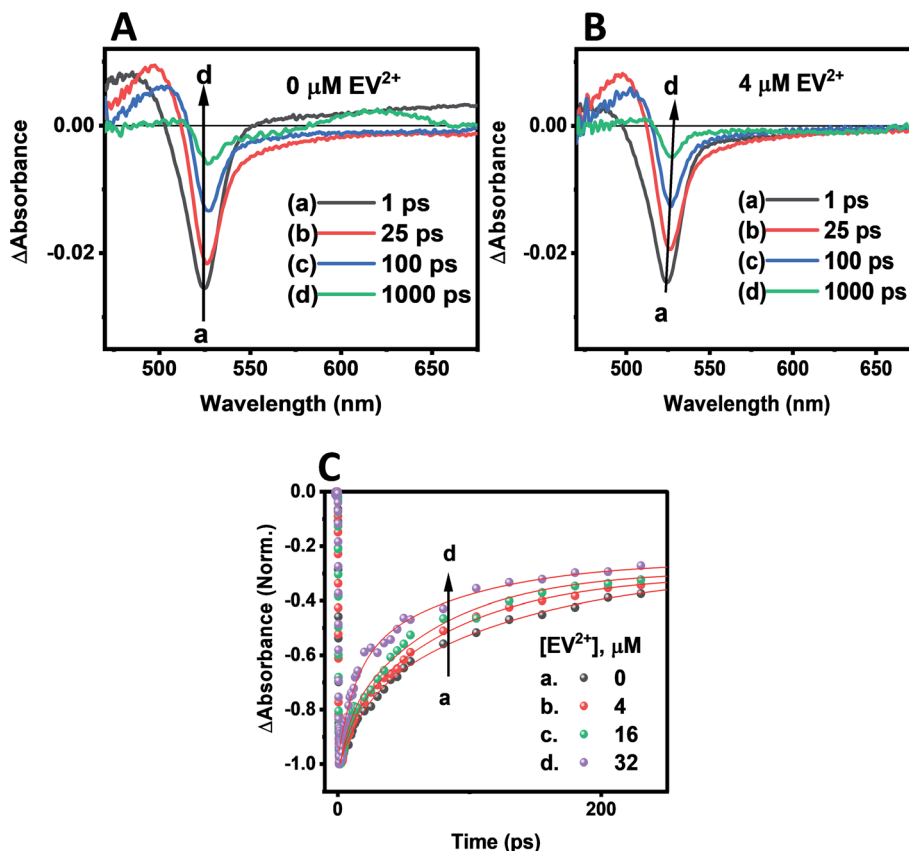
Fig. 5 Transient absorption spectra of CsPbBr$_3$–CdS suspension in toluene ($\approx$16 nM): (A) without EV^{2+} and (B) with 4 μM EV^{2+}. The difference absorption spectra were recorded following a 400 nm laser pulse (16 μJ cm^{-2}) excitation. (C) Kinetic traces of the CsPbBr$_3$–CdS bleach recovery at 527 nm in the absence and increasing concentrations of EV^{2+}.

the electron mediation of CdS in promoting interfacial electron transfer in the heterostructure (Scheme 1C).

Steady state photolysis and Fermi level equilibration

Although there have been several studies that demonstrate the photocatalytic properties through product identification,[17,18,36,61] direct spectroscopic identification of intermediates or electron transfer products is rather limited. If indeed the CsPbBr$_3$–CdS heterostructure is responsible for photocatalytic

reduction, we should be able to observe the buildup of stable viologen radical under continuous photoirradiation.[62,63]

Deaerated CsPbBr$_3$–CdS nanocrystal suspensions in toluene : ethanol (85 : 15 v/v%) mixed solvent containing 100 μM of EV^{2+} were subjected to steady-state visible light illumination (>400 nm; 200 mW cm^{-2}). Absorbance spectra were recorded periodically during the steady state photolysis experiment. Fig. 6A shows a representative difference absorbance spectrum, which shows distinct peaks at 405 nm and 608 nm,
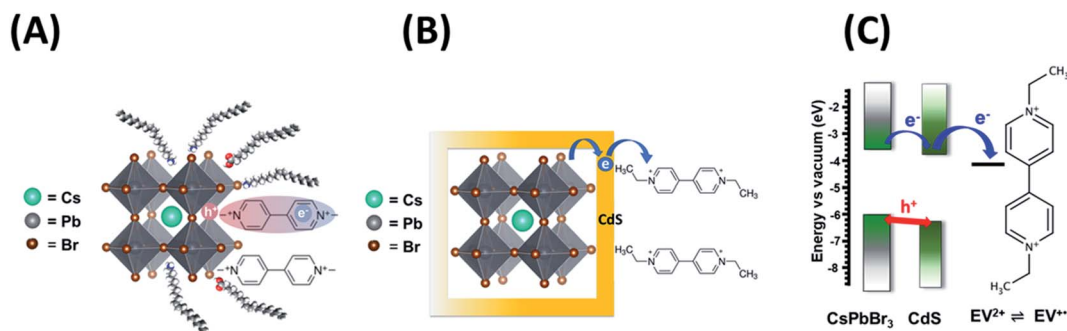
Scheme 1 Photoinduced electron transfer between CsPbBr$_3$ and viologen (A) without and (B) with mediation through a CdS layer. (C) Energetic diagram showing the flow of charge carriers and CdS mediated reduction of viologen.
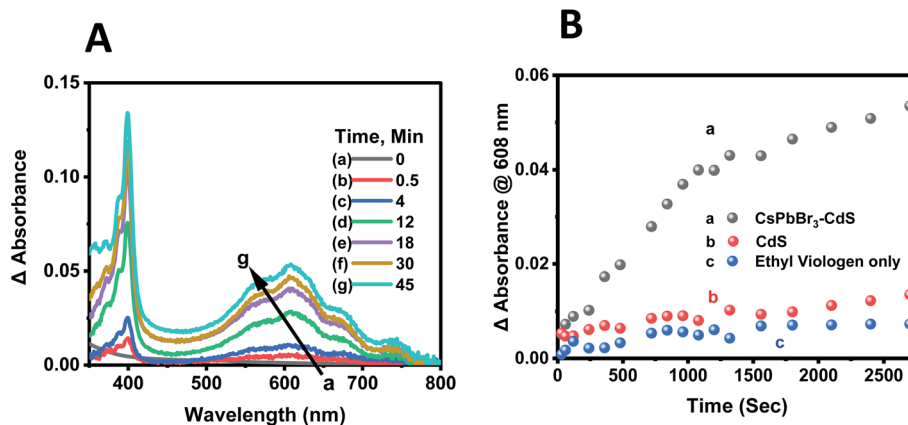
Fig. 6 (A) Difference absorbance spectra recorded during steady state photolysis corresponding to $EV^{+\bullet}$ formation. The $[CsPbBr_3-CdS + EV^{2+}]$ sample before excitation was used as a reference. Absorption spectra were recorded at different light exposure times. (B) Evolution of $EV^{+\bullet}$ formation monitored *via* the growth of absorbance at 608 nm with $CsPbBr_3$–CdS. Control experiments with CdS photocatalyst and in the absence of any photocatalyst are also shown. The initial concentration of EV^{2+} was 100 μM. Experiments were carried out in deaerated toluene/ethanol 85 : 15 v/v% with visible light excitation (Xe lamp, 400 nm long pass filter, 200 mW cm^{-2}).

corresponding to the absorbance of $EV^{+\bullet}$.[64] Fig. 6B shows the growth of the 608 nm absorption over time, which attains a plateau after about 45 minutes. The steady state concentration of $EV^{+\bullet}$ increased with increasing concentration of EV^{2+}. From the extinction coefficient of $EV^{+\bullet}$ at 608 nm ($\varepsilon = 1.4 \times 10^4$ M^{-1} cm^{-1})[63,64] we can determine the steady state concentration of the electron transfer product. The quantum yield (QY) of $EV^{+\bullet}$ formation ($\Phi_{EV^{+\bullet}}$) was determined using potassium ferrioxalate actinometry.[51,65] Details of the actinometry experiments are presented in the ESI.† In the present case we obtain a maximum quantum efficiency ($\Phi_{EV^{+\bullet}}$) of 8.4% for the electron transfer. Although the initial electron transfer yield as monitored from the transient absorption could be as high as 73%,[15] the back-electron transfer during the steady state irradiation makes the net electron transfer yield lower than the value obtained immediately after laser pulse excitation.

The steady state concentration of the reduction product $EV^{+\bullet}$ is dictated by the forward and back electron transfer processes. Because of the use of ethanol as a hole scavenger, the back electron transfer rate constant (k_{bet}) is significantly lower in the present experiments. The redox couple in contact with a semiconductor surface undergoes Fermi level equilibration that is dependent on the position of the conduction band and the potential of the redox couple. The equilibrium concentration of the reduced and oxidized species can be used to determine the flat band potential of the semiconductor. The steady state concentration of $[EV^{+\bullet}]_{ss}$ is indicative of charge equilibration between the $CsPbBr_3$–CdS nanocrystals and $EV^{2+}/EV^{+\bullet}$ couple. We employed the Nernst equation (expression (6)) to obtain the flat band potential of the $CsPbBr_3$–CdS heterostructure.

$$E_{CB} = E_{FB} = E^{\circ} - \left(\frac{0.059}{n}\right)\log\frac{[EV^{+\bullet}]_{ss}}{[EV^{2+}]_0 - [EV^{+\bullet}]_{ss}} \quad (6)$$

By substituting the redox potential of the $EV^{2+}/EV^{+\bullet}$ couple, $E^{\circ} = -0.449$ V *vs.* NHE,[64] and the steady state concentration values of the $EV^{+\bullet}$ (3.65 μM) and EV^{2+} ($[EV^{2+}] = [EV^{2+}]_0 - [EV^{+\bullet}]_{ss}$

= 96.35 μM), we obtain $E_{FB} = -0.365$ V *vs.* NHE. It is evident that the close lying conduction band potential of the $CsPbBr_3$–CdS heterostructure limits the one electron transfer to EV^{2+} (Scheme 1C). It should be noted that the flat band potential of the $CsPbBr_3$–CdS heterostructure obtained in this study is based on the charge equilibration between the semiconductor QD and redox couple and may differ from the values obtained from theoretical estimates or bulk material. The estimate of flat band potential provides an estimate of the energetics of the $CsPbBr_3$–CdS heterostructure suspended in the solvent medium to execute photocatalytic processes.

Conclusions

The design of $CsPbBr_3$–CdS heterostructure offers stabilization of perovskite nanocrystals for photocatalytic applications in polar medium. The salient feature of the $CsPbBr_3$–CdS heterostructure is realized through its stability in mixed solvents, remediation of surface defects, and increased emission yield. The stability of the $CsPbBr_3$ structure in mixed solvents with increased polarity has allowed us to accumulate electron transfer product (reduced viologen) under steady state irradiation conditions with a quantum efficiency of 8.4%. The relatively high electron transfer efficiency observed in the present study shows how a heterostructure design of perovskite nanocrystals plays a crucial role in dictating the photocatalytic properties of stable perovskite nanocrystals.

Data availability

The data is available within the main text and ESI.†

Author contributions

AK: conceptualization, synthesis, measurements, data analysis, validation, visualization, writing first draft and revision. JTD: data analysis, discussions, revision. JC: conceptualization of

material synthesis, preliminary investigation; revision. PVK: conceptualization, method development, funding acquisition, resources, supervision, discussions, writing.

Conflicts of interest

There are no conflicts to declare.

Acknowledgements

References

1 P. V. Kamat, Semiconductor Surface Chemistry as Holy Grail in Photocatalysis and Photovoltaics, *Acc. Chem. Res.*, 2017, **50**, 527–531.

2 Z. Xu, Z. Huang, T. Jin, T. Lian and M. L. Tang, Mechanistic Understanding and Rational Design of Quantum Dot/ Mediator Interfaces for Efficient Photon Upconversion, *Acc. Chem. Res.*, 2021, **54**, 70–80.

3 D. A. Hines and P. V. Kamat, Recent Advances in Quantum Dot Surface Chemistry, *ACS Appl. Mater. Interfaces*, 2014, **6**, 3041–3057.

4 Q. Shang, B. D. Piercy, M. D. Losego and T. Lian, Effect of Surface Ligand on Charge Separation and Recombination at CsPbI$_3$ Perovskite Quantum Dot/TiO$_2$ Interfaces, *J. Phys. Chem. C*, 2019, **123**, 21415–21421.

5 S. R. Smock, Y. Chen, A. J. Rossini and R. L. Brutchey, The Surface Chemistry and Structure of Colloidal Lead Halide Perovskite Nanocrystals, *Acc. Chem. Res.*, 2021, **54**, 707–718.

6 C. Murray, D. Norris and M. Bawendi, Synthesis and Characterization of Nearly Monodisperse CdE (E = S, Se, Te) Semiconductor, *J. Am. Chem. Soc.*, 1993, **115**, 8706–8715.

7 P. Alivisatos, Perspectives on the Physical Chemistry of Semiconductor Nanocrystals, *J. Phys. Chem.*, 1996, **100**, 13226–13239.

8 M. Nirmal and L. Brus, Luminescence Photophysics in Semiconductor Nanocrystals, *Acc. Chem. Res.*, 1999, **32**, 407–414.

9 J. Shamsi, A. S. Urban, M. Imran, L. De Trizio and L. Manna, Metal Halide Perovskite Nanocrystals: Synthesis, Post-Synthesis Modifications, and Their Optical Properties, *Chem. Rev.*, 2019, **119**, 3296–3348.

10 Y. Wu, X. Li and H. Zeng, Highly Luminescent and Stable Halide Perovskite Nanocrystals, *ACS Energy Lett.*, 2019, **4**, 673–681.

11 A. Dey, *et al.* State of the Art and Prospects for Halide Perovskite Nanocrystals, *ACS Nano*, 2021, **15**(7), 10775–10981.

12 S. T. Ha, R. Su, J. Xing, Q. Zhang and Q. H. Xiong, Metal Halide Perovskite Nanomaterials: Synthesis and Applications, *Chem. Sci.*, 2017, **8**, 2522–2536.

13 Y. L. Li, R. C. Lai, X. Luo, X. Liu, T. Ding, X. Lu and K. F. Wu, On the Absenceof a Phonon Bottleneck in Strongly Confined CsPbBr$_3$ Perovskite Nanocrystals, *Chem. Sci.*, 2019, **10**, 5983–5989.

14 S. M. Kobosko, J. T. DuBose and P. V. Kamat, Perovskite Photocatalysis. Methyl Viologen Induces Unusually Long-Lived Charge Carrier Separation in CsPbBr$_3$ Nanocrystals, *ACS Energy Lett.*, 2020, **5**, 221–223.

15 J. T. DuBose and P. V. Kamat, Surface Chemistry Matters. How Ligands Influence Excited State Interactions between CsPbBr$_3$ and Methyl Viologen, *J. Phys. Chem. C*, 2020, **124**, 12990–12998.

16 J. T. DuBose and P. V. Kamat, Probing Perovskite Photocatalysis. Interfacial Electron Transfer between CsPbBr$_3$ and Ferrocene Redox Couple, *J. Phys. Chem. Lett.*, 2019, **10**, 6074–6080.

17 H. Huang, B. Pradhan, J. Hofkens, M. B. J. Roeffaers and J. A. Steele, Solar-Driven Metal Halide Perovskite Photocatalysis: Design, Stability, and Performance, *ACS Energy Lett.*, 2020, **5**, 1107–1123.

18 J. S. Martin, *et al.* A Nanocrystal Catalyst Incorporating a Surface Bound Transition Metal to Induce Photocatalytic Sequential Electron Transfer Events, *J. Am. Chem. Soc.*, 2021, **143**, 11361–11369.

19 H. Huang, *et al.* Efficient and Selective Photocatalytic Oxidation of Benzylic Alcohols with Hybrid Organic–Inorganic Perovskite Materials, *ACS Energy Lett.*, 2018, **3**, 755–759.

20 Q. Li and T. Lian, Ultrafast Charge Separation in Two-Dimensional CsPbBr$_3$ Perovskite Nanoplatelets, *J. Phys. Chem. Lett.*, 2019, **10**, 566–573.

21 S. Shyamal and N. Pradhan, Halide Perovskite Nanocrystal Photocatalysts for CO$_2$ Reduction: Successes and Challenges, *J. Phys. Chem. Lett.*, 2020, **11**, 6921–6934.

22 D. Gerion, F. Pinaud, S. C. Williams, W. J. Parak, D. Zanchet, S. Weiss and A. P. Alivisatos, Synthesis and Properties of Biocompatible Water-Soluble Silica-Coated CdSe/ZnS Semiconductor Quantum Dots, *J. Phys. Chem. B*, 2001, **105**, 8861–8871.

23 D. V. Talapin, A. L. Rogach, A. Kornowski, M. Haase and H. Weller, Highly Luminescent Monodisperse CdSe and CdSe/ZnS Nanocrystals Synthesized in a Hexadecylamine-Trioctylphosphine Oxide–Trioctylphospine Mixture, *Nano Lett.*, 2001, **1**, 207–211.

24 E. Ryu, S. Kim, E. Jang, S. Jun, H. Jang, B. Kim and S.-W. Kim, Step-Wise Synthesis of InP/ZnS Core–Shell Quantum Dots and the Role of Zinc Acetate, *Chem. Mater.*, 2009, **21**, 573–575.

25 T. Torimoto, T. Adachi, K.-i. Okazaki, M. Sakuraoka, T. Shibayama, B. Ohtani, A. Kudo and S. Kuwabata, Facile Synthesis of ZnS–AgInS$_2$ Solid Solution Nanoparticles for

a Color-Adjustable Luminophore, *J. Am. Chem. Soc.*, 2007, **129**, 12388–12389.

26 Q. Zhong, M. Cao, H. Hu, D. Yang, M. Chen, P. Li, L. Wu and Q. Zhang, One-Pot Synthesis of Highly Stable CsPbBr3@SiO$_2$ Core–Shell Nanoparticles, *ACS Nano*, 2018, **12**, 8579–8587.

27 J. Shi, W. Ge, J. Zhu, M. Saruyama and T. Teranishi, Core–Shell CsPbBr$_3$@CdS Quantum Dots with Enhanced Stability and Photoluminescence Quantum Yields for Optoelectronic Devices, *ACS Appl. Nano Mater.*, 2020, **3**, 7563–7571.

28 V. K. Ravi, S. Saikia, S. Yadav, V. V. Nawale and A. Nag, CsPbBr$_3$/ZnS Core/Shell Type Nanocrystals for Enhancing Luminescence Lifetime and Water Stability, *ACS Energy Lett.*, 2020, **5**, 1794–1796.

29 W. Chen, J. Hao, W. Hu, Z. Zang, X. Tang, L. Fang, T. Niu and M. Zhou, Enhanced Stability and Tunable Photoluminescence in Perovskite CsPbX3/ZnS Quantum Dot Heterostructure, *Small*, 2017, **13**, 1604085.

30 H. Huang, B. Chen, Z. Wang, T. F. Hung, A. S. Susha, H. Zhong and A. L. Rogach, Water Resistant CsPbX$_3$ Nanocrystals Coated with Polyhedral Oligomeric Silsesquioxane and Their Use as Solid State Luminophores in All-Perovskite White Light-Emitting Devices, *Chem. Sci.*, 2016, **7**, 5699–5703.

31 J. Pan, *et al.* Bidentate Ligand-Passivated CsPbI3 Perovskite Nanocrystals for Stable Near-Unity Photoluminescence Quantum Yield and Efficient Red Light-Emitting Diodes, *J. Am. Chem. Soc.*, 2018, **140**, 562–565.

32 H. Huang, B. K. Chen, Z. G. Wang, T. F. Hung, A. S. Susha, H. Z. Zhong and A. L. Rogach, Water Resistant CsPbX$_3$ Nanocrystals Coated with Polyhedral Oligomeric Silsesquioxane and Their Use as Solid State Luminophores in All-Perovskite White Light-Emitting Devices, *Chem. Sci.*, 2016, **7**, 5699–5703.

33 M. Imran, B. T. Mai, L. Goldoni, M. Cirignano, H. B. Jalali, F. Di Stasio, T. Pellegrino and L. Manna, Switchable Anion Exchange in Polymer-Encapsulated APbX$_3$ Nanocrystals Delivers Stable All-Perovskite White Emitters, *ACS Energy Lett.*, 2021, **6**, 2844–2853.

34 P. V. Kamat, N. Pradhan, K. Schanze, P. S. Weiss, J. Buriak, P. Stang, T. W. Odom and G. Hartland, Challenges and Opportunities in Designing Perovskite Nanocrystal Heterostructures, *ACS Energy Lett.*, 2020, 2253–2255.

35 S. Bera and N. Pradhan, Perovskite Nanocrystal Heterostructures: Synthesis, Optical Properties, and Applications, *ACS Energy Lett.*, 2020, **5**, 2858–2872.

36 S. K. Dutta, S. K. Mehetor and N. Pradhan, Metal Semiconductor Heterostructures for Photocatalytic Conversion of Light Energy, *J. Phys. Chem. Lett.*, 2015, **6**, 936–944.

37 J. H. Bang and P. V. Kamat, Quantum Dot Sensitized Solar Cells. A Tale of Two Semiconductor Nanocrystals: CdSe and CdTe, *ACS Nano*, 2009, **3**, 1467–1476.

38 V. K. Ravi, G. B. Markad and A. Nag, Band Edge Energies and Excitonic Transition Probabilities of Colloidal CsPbX$_3$ (X = Cl, Br, I) Perovskite Nanocrystals, *ACS Energy Lett.*, 2016, **1**, 665–671.

39 Q. A. Akkerman, *et al.* Strongly Emissive Perovskite Nanocrystal Inks for High-Voltage Solar Cells, *Nat. Energy*, 2016, **2**, 16194.

40 P. Cottingham and R. L. Brutchey, On the Crystal Structure of Colloidally Prepared CsPbBr$_3$ Quantum Dots, *Chem. Commun.*, 2016, **52**, 5246–5249.

41 J. Zhang, S. Wageh, A. Al-Ghamdi and J. Yu, New Understanding on the Different Photocatalytic Activity of Wurtzite and Zinc-Blende CdS, *Appl. Catal., B*, 2016, **192**, 101–107.

42 A. Demortière, *et al.* Strain-Driven Stacking Faults in CdSe/CdS Core/Shell Nanorods, *J. Phys. Chem. Lett.*, 2018, **9**, 1900–1906.

43 L. Protesescu, S. Yakunin, M. I. Bodnarchuk, F. Krieg, R. Caputo, C. H. Hendon, R. X. Yang, A. Walsh and M. V. Kovalenko, Nanocrystals of Cesium Lead Halide Perovskites (CsPbX$_3$, X = Cl, Br, and I): Novel Optoelectronic Materials Showing Bright Emission with Wide Color Gamut, *Nano Lett.*, 2015, **15**, 3692–3696.

44 S. Bhaumik, S. A. Veldhuis, Y. F. Ng, M. Li, S. K. Muduli, T. C. Sum, B. Damodaran, S. Mhaisalkar and N. Mathews, Highly Stable, Luminescent Core–Shell Type Methylammonium–Octylammonium Lead Bromide Layered Perovskite Nanoparticles, *Chem. Commun.*, 2016, **52**, 7118–7121.

45 K. Xu, C. C. Lin, X. Xie and A. Meijerink, Efficient and Stable Luminescence from Mn^{2+} in Core and Core–Isocrystalline Shell CsPbCl$_3$ Perovskite Nanocrystals, *Chem. Mater.*, 2017, **29**, 4265–4272.

46 V. K. Ravi, R. A. Scheidt, J. DuBose and P. V. Kamat, Hierarchical Arrays of Cesium Lead Halide Perovskite Nanocrystals through Electrophoretic Deposition, *J. Am. Chem. Soc.*, 2018, **140**, 8887–8894.

47 Y. Zhao, C. Shen, L. Ding, J. Liu, W. Xiang and X. Liang, Novel B-site Cd^{2+} doped CsPbBr$_3$ Quantum Dot Glass Toward Strong Fluorescence and High Stability For wLED, *Opt. Mater.*, 2020, **107**, 110046.

48 S. Christodoulou, *et al.* Synthesis of Highly Luminescent Wurtzite CdSe/CdS Giant-Shell Nanocrystals Using a Fast Continuous Injection Route, *J. Mater. Chem. C*, 2014, **2**, 3439–3447.

49 L. Carbone, *et al.* Synthesis and Micrometer-Scale Assembly of Colloidal CdSe/CdS Nanorods Prepared by a Seeded Growth Approach, *Nano Lett.*, 2007, **7**, 2942–2950.

50 D. V. Talapin, J. H. Nelson, E. V. Shevchenko, S. Aloni, B. Sadtler and A. P. Alivisatos, Seeded Growth of Highly Luminescent CdSe/CdS Nanoheterostructures with Rod and Tetrapod Morphologies, *Nano Lett.*, 2007, **7**, 2951–2959.

51 V. L. Bridewell, R. Alam, C. J. Karwacki and P. V. Kamat, CdSe/CdS Nanorod Photocatalysts: Tuning the Interfacial Charge Transfer Process through Shell Length, *Chem. Mater.*, 2015, **27**, 5064–5071.

52 Z. Zhu, Q. Sun, Z. Zhang, J. Dai, G. Xing, S. Li, X. Huang and W. Huang, Metal Halide Perovskites: Stability and Sensing-Ability, *J. Mater. Chem. C*, 2018, **6**, 10121–10137.

53 X. Li, *et al.* All Inorganic Halide Perovskites Nanosystem: Synthesis, Structural Features, Optical Properties and Optoelectronic Applications, *Small*, 2017, **13**, 1603996.

54 L. J. Ruan, B. Tang and Y. Ma, Improving the Stability of $CsPbBr_3$ Nanocrystals in Ethanol by Capping with $PbBr_2$-Adlayers, *J. Phys. Chem. C*, 2019, **123**, 11959–11967.

55 P. V. Kamat, J. P. Chauvet and R. W. Fessenden, Photoelectrochemistry in Particulate Systems. 4. Photosensitization of a TiO_2 Semiconductor with a Chlorophyll Analogue, *J. Phys. Chem.*, 1986, **90**, 1389–1394.

56 J. R. Lakowicz, *Principles of Fluorescence Spectroscopy*. Springer, New York, 2006.

57 M. D. Peterson, S. C. Jensen, D. J. Weinberg and E. A. Weiss, Mechanisms for Adsorption of Methyl Viologen on CdS Quantum Dots, *ACS Nano*, 2014, **8**, 2826–2837.

58 K. Wu, G. Liang, Q. Shang, Y. Ren, D. Kong and T. Lian, Ultrafast Interfacial Electron and Hole Transfer from $CsPbBr_3$ Perovskite Quantum Dots, *J. Am. Chem. Soc.*, 2015, **137**, 12792–12795.

59 N. Mondal and A. Samanta, Complete Ultrafast Charge Carrier Dynamics in Photo-Excited All-Inorganic Perovskite Nanocrystals ($CsPbX_3$), *Nanoscale*, 2017, **9**, 1878–1885.

60 J. Aneesh, A. Swarnkar, V. Kumar Ravi, R. Sharma, A. Nag and K. V. Adarsh, Ultrafast Exciton Dynamics in Colloidal $CsPbBr_3$ Perovskite Nanocrystals: Biexciton Effect and Auger Recombination, *J. Phys. Chem. C*, 2017, **121**, 4734–4739.

61 D. Cardenas-Morcoso, A. F. Gualdrón-Reyes, A. B. Ferreira Vitoreti, M. García-Tecedor, S. J. Yoon, M. Solis de la Fuente, I. Mora-Seró and S. Gimenez, Photocatalytic and Photoelectrochemical Degradation of Organic Compounds with All-Inorganic Metal Halide Perovskite Quantum Dots, *J. Phys. Chem. Lett.*, 2019, **10**, 630–636.

62 F. Zhao, Q. Li, K. Han and T. Lian, Mechanism of Efficient Viologen Radical Generation by Ultrafast Electron Transfer from CdS Quantum Dots, *J. Phys. Chem. C*, 2018, **122**, 17136–17142.

63 C. T. Harris and P. V. Kamat, Photocatalysis with CdSe Nanoparticles in Confined Media: Mapping Charge Transfer Events in the Subpicosecond to Second Timescales, *ACS Nano*, 2009, **3**, 682–690.

64 C. L. Bird and A. T. Kuhn, Electrochemistry of the Viologens, *Chem. Soc. Rev.*, 1981, **10**, 49–82.

65 C. G. Hatchard and C. A. Parker, A New Sensitive Chemical Actinometer – II. Potassium Ferrioxalate as a Standard Chemical Actinometer, *Proc. R. Soc. London, Ser. A*, 1956, **235**, 518–536.